Solution NMR Structure and X-ray Absorption Analysis of the C-Terminal Zinc-Binding Domain of the SecA ATPase[†]

Brian R. Dempsey,[‡] Mark Wrona,[‡] Jana M. Moulin,[‡] Gregory B. Gloor,[‡] Farideh Jalilehvand,[§] Gilles Lajoie,[‡] Gary S. Shaw,[‡] and Brian H. Shilton*[,‡]

Department of Biochemistry, University of Western Ontario, London ON N6A 5C1, Ontario, Canada, and Department of Chemistry, University of Calgary, 2500 University Drive Northwest, Calgary AB T2N 1N4, Alberta, Canada

Received April 7, 2004; Revised Manuscript Received May 24, 2004

ABSTRACT: The solution NMR structure of a 22-residue Zn^{2+}-binding domain (ZBD) from *Escherichia coli* preprotein translocase subunit SecA is presented. In conjunction with X-ray absorption analysis, the NMR structure shows that three cysteines and a histidine in the sequence $CXCXSGX_8CH$ assume a tetrahedral arrangement around the Zn^{2+} atom, with an average $Zn^{2+}-S$ bond distance of 2.30 Å and a $Zn^{2+}-N$ bond distance of 2.03 Å. The NMR structure shows that ND1 of His20 binds to the Zn^{2+} atom. The $ND1-Zn^{2+}$ bond is somewhat strained: it makes an angle of approximately 17° with the plane of the ring, and it also shows a significant "in-plane" distortion of 13°. A comprehensive sequence alignment of the SecA-ZBD from many different organisms shows that, along with the four Zn^{2+} ligands, there is a serine residue (Ser12) that is completely conserved. The NMR structure indicates that the side chain of this serine residue forms a strong hydrogen bond with the thiolate of the third cysteine residue (Cys19); therefore, the conserved serine appears to have a critical role in the structure. SecB, an export-specific chaperone, is the only known binding partner for the SecA-ZBD. A phylogenetic analysis using 86 microbial genomes shows that 59 of the organisms carry SecA with a ZBD, but only 31 of these organisms also possess a gene for SecB, indicating that there may be uncharacterized binding partners for the SecA-ZBD.

In bacteria, many proteins must be translocated across the cell membrane to function in cell wall biosynthesis, transport, and signaling. Preprotein translocase, otherwise known as the "general secretory system", is the essential multicomponent system that catalyzes most translocation across the cell membrane. The central components of preprotein translocase are SecYEG, an integral membrane complex, and SecA, a peripheral ATPase (*1*). In the presence of the substrate preprotein, these two components form a complex and push the preprotein through the membrane by multiple cycles of ATP hydrolysis (*2*).

One of the requirements of the translocation reaction is that the preprotein must be unfolded. To meet this requirement, many cells express an export-specific chaperone called SecB. SecB is a homotetramer that binds unfolded preproteins and maintains them in a transport-competent state. SecB and SecA are able to form a complex, and it is thought that SecB delivers the preprotein to SecA (*3*); in addition, interaction with SecB stimulates SecA ATPase activity (*4*, *5*).

The extreme C-terminus of *Escherichia coli* SecA harbors a Zn^{2+}-binding domain (ZBD) that is critical for the interaction between SecA and SecB (*6*−*8*). The structures of SecA from *Bacillus subtilis* (*9*) and *Mycobacterium tuberculosis* (*10*) have been solved, but the ZBD of the *B. subtilis* SecA was absent from the structure, and *M. tuberculosis* SecA does not contain a ZBD. The interaction between SecA and SecB is important for understanding how preprotein is delivered from the ribosome to the translocon, and our knowledge of this interaction was advanced by the recent crystal structure of *Haemophilus influenzae* SecB with bound ZBD (*11*). The ZBD adopts a novel fold, binding to a region of the SecB tetramer that agrees with results from earlier mutagenesis studies (*12*, *13*). In the structure of the complex, the Zn^{2+} atom is coordinated by the thiolates of Cys8, Cys10, and Cys19, and the imidazole moiety of His20; contacts with the surface of SecB are mediated entirely by hydrophilic side chains, many of which are at the N- and C-terminal portions of the ZBD, outside of the regions directly stabilized by Zn^{2+} ligation; therefore, these regions may assume a different conformation when the ZBD is not bound to SecB. The crystal structure, which was refined

[†] This research was supported by the Canadian Institutes of Health Research (CIHR) operating grants MOP-57668 (B.H.S.) and FRN11374 (G.B.G.), CIHR operating and multi-user maintenance grants (G.S.S.), the Canada Research Chairs Program (G.S.S.), the Natural Sciences and Engineering Research Council (G.L.), and the Ontario Research and Development Challenge Fund (G.L.). X-ray absorption spectroscopic studies were supported by the Alberta Synchrotron Institute (F.J.). The EXAFS experiment was conducted under the approval of the Photon Factory Program Advisory Committee (proposal No. 2003G286). B.R.D. is the recipient of an Ontario Graduate Scholarship.

* To whom correspondence should be addressed. Telephone: (519) 661-4124. Fax: (519) 661-3175. E-mail: bshilton@uwo.ca.

[‡] University of Western Ontario.

[§] University of Calgary.

[1] Abbreviations: ZBD, zinc-binding domain; XANES, X-ray absorption near-edge structure; EXAFS, X-ray absorption fine structure; ESI-MS, electrospray ionization mass spectroscopy; TCEP, tris(2-carboxyethyl)phosphine.

10.1021/bi0493057 CCC: $27.50
Published on Web 06/29/2004

to a resolution of 2.8 Å, shows that the Zn^{2+}−imidazole bond makes an angle of approximately 20° with respect to the plane of the imidazole ring. However, His20 shows a relatively high temperature factor, and distance restraints between the Zn^{2+} and ligating atoms were applied during refinement of the crystal structure, indicating that there may be some uncertainty in the conformation of His20. Additionally, a strictly conserved serine residue was modeled as an alanine for reasons that are not clear.

To gain further insight into the solution structure and Zn^{2+}-binding chemistry of the ZBD, we describe a high-resolution NMR structure for the ZBD of *E. coli* SecA. We show that the ZBD has no defined structure in the absence of Zn^{2+} ions. Coordination around the Zn^{2+} center was investigated using extended X-ray absorption fine structure (EXAFS) analysis on the Zn^{2+}-bound peptide. The EXAFS data allowed us to apply experimental restraints on the Zn^{2+}−S and Zn^{2+}−N bond distances. Surprisingly, the NMR structure of the ZBD shows that the N- and C-termini retain their conformation in solution; in other words, the ZBD does not undergo a large conformational change when it binds to SecB. We find that the ligating histidine (His20) binds the Zn^{2+} atom using its ND1 nitrogen, but that the imidazole ring is not in an ideal conformation to make a low energy Zn^{2+}−N bond, presumably because His20 is adjacent to Cys19, another Zn^{2+}-ligating residue. Our analysis indicates that Zn^{2+} coordination is supported by a series of "second-sphere" interactions; in particular, the NMR data indicate that Ser12 forms a strong hydrogen bond with one of the Zn^{2+}-ligating thiolates. Such second-shell coordinating interactions have been catalogued for a variety of Zn^{2+}-binding motifs (*14*), but the complete conservation of Ser12 in the SecA-ZBD suggests that it has a critical role for proper Zn^{2+} ligation and folding.

SecB is the only known binding partner for the ZBD of SecA; however, we have analyzed available bacterial genomes and found that the ZBD is frequently present even in organisms that do not possess a gene for SecB, suggesting that the ZBD has binding partners other than SecB.

EXPERIMENTAL PROCEDURES

Genetic Analysis. We produced a custom sequence database containing the predicted proteomes of 111 organisms derived from completely sequenced genomes of bacteria, archaebacteria, and eukaryotes. PSI-BLAST (*15*), initiated with representative protein sequences and with an *E* value cutoff of 0.005, was used to gather all SecA and SecB sequences. Multiple sequence alignments were generated by MAFFT (*16*) and CLUSTAL (*17*), and were edited and compared using Jalview (www.jalview.org). In the end, 86 SecA protein homologues and 32 SecB homologues were used. In most cases, each sequence occurred only once per organism. All were from either eubacteria or eukaryotic organelles.

Preparation of Zinc-Binding Peptide for NMR Studies. The SecA C-terminal Zn^{2+}-binding domain was prepared by solid-phase synthesis using the FMOC protocol, and was purified by reversed phase HPLC. The peptide has a mass of 2459.22 Da, determined by electrospray mass spectrometry. NMR samples were made up in either 90/10 H_2O/D_2O or 100% D_2O. Peptide concentrations of 1.7 and 3.5 mM were used. The buffer consisted of 20 mM deuterated Pipes pH 7.0, 50 mM NaCl, 5 mM NaN_3, 0.5 mM TCEP, and a 2-fold excess of $ZnCl_2$ to peptide. DSS (sodium 2,2-dimethyl-, 2-silapentane-5-sulfonate) was added as an internal NMR standard.

NMR Spectroscopy. All NMR spectra were carried out on Varian Unity 500 or Varian Inova 600 MHz spectrometers at 25 °C using 5 mm triple-resonance ^1H, ^{13}C, ^{15}N probes. Sequence specific assignments were completed using DQF-COSY (*18*) and TOCSY (*19*) experiments in both 90% H_2O/10% D_2O and 99.95% D_2O. In all cases, water suppression was accomplished using a weak 2 s presaturation pulse of the H_2O resonance. TOCSY experiments were collected using a MLEV-17 spin-lock mixing period of 50 ms. NOESY spectra were collected using the hypercomplex method with mixing times of 300 ms and 75 ms (*20*). Typical data sets comprised 32 or 48 transients and 512 increments for spectral widths of either 5200 or 6200 Hz. All data were processed using NMRPipe (*21*) and VNMR 6.1C software using a 60° shifted sine-bell squared function and zero filling to yield final digital resolutions of 5.1 Hz/point (F1) and 2.9 Hz/point (F2).

NMR Structure Calculations. Proton−proton distances in NOESY spectra in D_2O were calibrated by averaging all resolved Hβ1−Hβ2 cross-peaks from AMX spin systems and setting this distance to 1.78 Å. NOEs involving aromatic protons were calibrated using the δCH to ϵCH of Tyr16 and setting this distance to 2.46 Å. All NOEs from spectra in H_2O involving amide protons were calibrated according to methods of Gagné *et al.* (*22*) using in-house modified scripts for two-dimensional $^1H-^1H$ spectra.

Coupling constants for $^3J_{HN\alpha}$ were measured from high-resolution one-dimensional ^1H spectra and converted to ϕ angle restraints using the Karplus relationship (*23*, *24*). Psi (ψ) angle restraints for the $i-1$ residue were determined using the NOE ratio for $I\alpha^iN^i/I\alpha^{i-1}N^i$ residues (*22*). Ratios > 1 were assigned to a ψ angle of 120° ± 100°, while ratios < 1 were assigned a ψ of −60° ± 60°. A comparison of this method with ϕ, ψ angles derived using the program TALOS (*25*) with αCH and αH input yielded similar ϕ, ψ space restraints. Stereospecific assignment of AMX spin systems was accomplished using the methods of Wagner *et al.* (*26*) through comparison of relative NOE intensities between NH, αCH, and βCH_2 protons in 75 ms NOESY spectra and *J*-coupling patterns in DQF-COSY spectra. χ^1 angles for stereospecifically assigned residues were input as $\chi^1 \pm 30°$.

All structure calculations were carried out with CNS (*27*) using the standard anneal.inp input file. Typically, 100 structures were submitted for calculation, and the best 20 were chosen on the basis of residual NOE energy and geometry. All initial structures were calculated without Zn^{2+} ion restraints to verify the position and geometry of possible Zn^{2+} ligands. After the Zn^{2+} ligands had been identified, restraints were applied between the Zn^{2+} and SG atoms of Cys8, Cys10, and Cys19 (2.30 Å) and ND1 of His20 (2.03 Å), based on the EXAFS data. To impose tetrahedral geometry on the coordination, six additional distance restraints were applied: three distance restraints (3.75 Å) between the SG atoms of the cysteines and three distance restraints (3.60 Å) between the ND1 atom of His20 and each of the cysteine SG atoms. The coordinates for the 20 lowest

energy structures, calculated either with or without distance restraints to the Zn^{2+} atom, have been deposited in the PDB (*28*) with ID 1SX1 and 1SX0, respectively.

X-ray Absorption Analysis. The peptide (5.1 mg, 2.07 μmol) was dissolved in 1 mL of a buffer comprised of 50 mM Hepes, 1 mM TCEP, 32% glycerol, pH 7.5. To this solution was added 19.5 μL of 100 mM $Zn(OAc)_2$. The solution remained clear after the addition of $Zn(OAc)_2$ and was sterilized by passage through a 0.22 μm syringe filter. A few grains of 1,1,1-trichloro-2-methyl-2-propanol were added to the solution to inhibit microbial growth. The 2 mM ZBDsample was loaded into a 2 mm titanium cell with 63 μm Kapton windows.

The Zn K-edge X-ray absorption spectra were recorded using the focused beam at BL-12C at the Photon Factory of High Energy Accelerator Research Organization (Tsukuba, Japan), under dedicated conditions (2.5 GeV, 300 mA). Harmonics from the Si(111) double crystal monochromator were rejected using a rhodium coated focusing mirror. A RMC continuous-flow liquid helium cryostat maintained a constant sample temperature of 20 K.

The Zn K-edge XAS data were recorded in fluorescence mode by means of a liquid nitrogen cooled 19-element solid-state Ge detector array. The energy window of the detector elements was adjusted around the Zn K_α fluorescence line to reduce the background of scattered radiation. The signal from each detector channel was examined for each scan to confirm the absence of artifacts. A total of 15 scans (18 channels per scan) were then averaged (I_f) for the ZBD sample. The XAS spectrum was obtained as (I_f/I_0) versus energy, where I_0 is the incident beam intensity. The energy scale was externally calibrated by assigning the first inflection point of a zinc metal foil to 9659.0 eV measured before and after collecting the spectra.

The scans comprise 10 eV steps in the pre-edge region (9470−9600 eV), 0.35 eV in the edge region (9600−9720 eV), and 3 eV in the EXAFS region (9720−10 700 eV), with 2 s of integration time for each step. The total integration time per scan was 28 min, with 7 h of total exposure time. A comparison of the first and last scan showed no evidence of radiation damage.

The EXAFS oscillation was extracted using the WinXAS version 3.2 program system (*29*). The background absorption was subtracted using a first-order polynomial over the pre-edge region, followed by normalization of the edge step. The energy scale was converted to *k*-space, where $k = (8\pi^2 m_e/h^2)(E - E_0)$, using a threshold energy of $E_0 = 9661.5$ eV. Above the edge, the atomic background contribution was removed by subtracting an 8-region cubic spline. The least-squares refinements were performed using both raw data ($k = 2.5-15.1$ Å^{-1}) and Fourier-filtered data, for which the EXAFS data were Fourier transformed over different *k*-ranges, followed by back-transformation over the *r*-ranges given in Table 3.

The EXAFS oscillation, $\chi(k)$, can be modeled using the expression:

$$\chi(k) = \sum_i \frac{N_i \cdot {S_0}^2(k)}{k \cdot {R_i}^2} |f_{\text{eff}}(k)|_i \cdot \exp(-2k^2\sigma_i^2) \cdot \exp[-2R_i/\Lambda(k)] \cdot \sin[2kR_i + \phi_{ij}(k)] \quad (1)$$

Table 1: NMR Structure Parameters

parameter	ZBD[a] (NOE restraints only)	ZBD-Zn[a] (NOE restraints and Zn^{2+}-coordination restraints)
NOE distance restraints (total)	274	274
intraresidue	121	121
sequential	65	65
short range	32	32
long range	56	56
zinc restraints	0	10
dihedral angle restraints	33	33
ϕ	11	11
ψ	16	16
χ^1	6	6
stereospecific assignments	9	9
NOE violations[a]	0	0
avg. CNS energies (kcal/mol)[a]		
total energy	28.71 ± 2.58	30.23 ± 2.71
NOE energy	0.92 ± 0.29	1.05 ± 0.54
Ramachandran statistics[a]		
favored	75.4%	79.6%
allowed	18.6%	15.7%
generously allowed	6.1%	4.6%
disallowed	0.0%	0.0%
RMSD to mean structure (Å)[a] residues 2−20		
backbone atoms	0.21 ± 0.03	0.19 ± 0.03
heavy atoms	0.73 ± 0.05	0.72 ± 0.06

[a] The coordinates for the 20 lowest energy structures, calculated either with or without distance restraints to the Zn^{2+} atom, have been deposited in the PDB (*28*) with ID 1SX1 and 1SX0, respectively.

Table 2: Conservation in the ZBD of SecA

position	residue	conservation[a]	changes[b]
1	K	42	4T,4Q,2H,2N,2G,I,E,D
2	V,I,L	55	2T,2P
3	G	45	4S,3K,2A,2E,P,H,N
4	R	57	A,K
5	N	58	D
6	D,E	52	4A,2T,G
7	P	50	2L,3A,2K,D,S
8	C	59	
9	P	52	2W,2K,Y,F,H
10	C	59	
11	G	57	K,Q
12	S	59	
13	G	59	
14	K	56	2L,M
15	K	58	P
16	Y,F	59	
17	K	58	E
18	Q,N	33	15H,3Y,2K,2D,VEMS
19	C	59	
20	H	47	12C
21	G	58	1A
22	R,K	30	12Q,6A,4S,3I,2L,2V

[a] Number of sequences (out of the 59 ZBD-containing SecA molecules) in which residue(s) in the first column occur. [b] Number and nature of amino acid changes at a given position.

The parameters in the above equation are as follows: the number N_i of backscattering atoms at the mean distance R_i from the absorber in the *i*th shell; the Debye−Waller parameter σ_i^2 related to the mean-square variation in a Gaussian distribution of distances around R_i; the scattering variable *k*; the effective amplitude function $|f_{\text{eff}}(k)|_i$; the total phase-shift $\phi_{ij}(k)$ of the absorber−scatterer pair; the photoelectron mean free path $\lambda(k)$; and the amplitude reduction factor ${S_0}^2(k)$.

Table 3: Determination of Zn^{2+}-ZBD Coordination Parameters by EXAFS[a]

fit	*k*-range (Å^{-1})	FT-filter *r*-range (Å)	coordination no.[b]	*R* (Å)[c]	σ^2 (Å^2)[d]	S_0^2	$\mathscr{R}$ [e]
1	2.5−15.1	1.0−2.5	**1** N	2.03	0.4	0.99	12.0
			3 S	2.30	4.3		
2	2.5−14.1	1.0−2.5	**1** N	2.03	2.0	1.07	11.1
			3 S	2.30	4.9		
3	2.5−12.7	0.9−2.4	**1** N	2.03	2.0	1.00	10.9
			3 S	2.29	4.5		
4	2.5−15.1	unfiltered	**1** N	2.03	0.4	1.00	26.1
			3 S	2.30	4.2		

[a] Curve-fitting results for zinc K-edge EXAFS k^3 data of Zn^{2+}-ZBD. [b] Parameter values in bold are held constant. [c] Zn−backscatterer distance. [d] Debye−Waller factor × 10^3. [e] Residual.

The $\chi(k)$ model function was constructed using the *ab initio* calculated amplitude $f_{eff}(k)_i$, phase shift $\phi_{ij}(k)$, and mean free path $\lambda(k)$ functions by means of the FEFF (7.02) program (*30*). In our least-squares refinements of the k^3-weighted EXAFS data, the coordination numbers were fixed according to the $Zn^{2+}-S_3N$ model, allowing *R*, σ^2, and ΔE_0 to float. ΔE_0 values varied between 4.7 and 5.6. $S_0^2(k)$ was refined, except when $k_{max} < 13$ Å^{-1}, yielding values of about 1.0 (Table 3). The accuracy of the bond distances *R* is within ±0.02 Å.

RESULTS

Sequence and Phylogenetic Analysis of the C-Terminal Domain of SecA. The sequence alignment of the ZBD (Figure 1) shows that the four putative Zn^{2+}-coordinating amino acids (Cys885, Cys887, Cys896, and His897 in *E. coli* ZBD) are conserved (the histidine is sometimes replaced by cysteine, which could also function to coordinate Zn^{2+}). The ZBD sequence is intriguing for a number of reasons. First, the spacing between the Zn^{2+}-coordinating residues is extremely short − there is only one residue, almost always a proline, between the first two cysteines, and the second two Zn^{2+}-coordinating residues are always next to each other in the sequence, which is rare for zinc fingers and other Zn^{2+}-binding motifs, and in fact there are no examples of a Zn^{2+}-coordinating motif in which the ligating cysteine and histidine residues are adjacent to each other. Furthermore, there are always exactly 8 residues between the two pairs of putative Zn^{2+}-coordinating residues. There are several other conserved amino acids in addition to the residues thought to be Zn^{2+} ligands; these include a Gly−Ser−Gly motif, several basic residues, and an aromatic residue. This raises a second intriguing property of the ZBD, which is its extremely high overall sequence conservation. The compact nature of the motif may dictate a low tolerance for amino acid substitutions; alternatively, the high degree of sequence conservation could indicate a conserved interaction with other macromolecules.

SecB is an export-specific chaperone (*31*), and a function of the ZBD on SecA is to engage preprotein-bound SecB, thereby directing the preprotein to transloci at the membrane (*3*, *7*). We used the available microbial genome sequences to investigate whether the presence of SecB was correlated with the presence of the ZBD on SecA. SecA is present in all of the sequenced genomes, consistent with its essential role in translocation (*32*). With the expanded number of fully sequenced genomes, it is clear that SecB is found only in diderm organisms (organisms with an outer membrane (*33*); Figure 2). We found that in all of the SecB-containing organisms (31 out of 86 genomes analyzed), the SecA molecule contained a ZBD, consistent with the observation that SecB function is dependent on the presence of the ZBD in SecA (*7*). On the other hand, organisms that did not contain SecB (55 out of 86 genomes analyzed) were evenly divided between those that have a SecA with a conserved ZBD (28 organisms) and those with SecA lacking the ZBD (27 organisms). Of the organisms represented in the alignment in Figure 1, only *E. coli* and *M. loti* have SecB in their genome; therefore, the presence and high conservation of the SecA-ZBD in organisms that lack SecB suggests that the domain has other, as yet uncharacterized functions.

Solution Structure of the SecA Zinc-Binding Domain. A previous 2.8 Å resolution crystal structure was determined for a complex of the SecA-ZBD and SecB from *Haemophilus influenzae*; we have determined the solution structure of the isolated *Esherichia coli* SecA-ZBD using two-dimensional ^{1}H NMR spectroscopy. The peptide used for the structure analysis was produced by solid-phase synthesis using unlabeled amino acids and comprised the C-terminal 22 residues from *E. coli* SecA, residues 879−901: KVGRND-PCPCGSGKKYKQCHGR. In the interest of simplicity, and because the length of the linker region is variable in SecA molecules, we will refer to the N-terminal lysine of the *E. coli* ZBD as residue 1.

Zn^{2+} is required for folding of the ZBD, as indicated by one-dimensional ^{1}H NMR spectra recorded for the ZBD in the absence and presence of Zn^{2+} (Figure 3). The spectrum recorded in the absence of Zn^{2+} (Figure 3A) has sharp resonances and little dispersion, indicating that the amino acids of the peptide are sampling many different environments, as expected for unfolded peptide. Upon the addition of 2 equiv of Zn^{2+} (Figure 3B), a second set of resonances appears consistent with Zn^{2+}-binding in the slow-exchange regime. These resonances are more well resolved, indicating that the peptide adopts a stable, folded conformation.

The complete sequential assignment for the Zn^{2+}-bound ZBD was carried out using standard two-dimensional ^{1}H NMR experiments. In particular, the well-resolved chemical shifts allowed us to assign all but 5 of 131 nonexchanging protons from the 22 residue ZBD. In addition, stereospecific assignments for the AMX spin-systems N5, D6, C8, C10, Y16, and C19 were used to obtain χ^1 angle information used in structure calculations. The solution structure of ZBD was determined using 274 distance restraints and 33 angular (ϕ,ψ,χ^1) restraints. No hydrogen-bonding restraints were used. Because NMR experiments did not identify Zn^{2+}−protein interactions, initial structure calculations did not include restraints related to metal ion coordination. From a family of 100 structures, the 20 lowest energy structures having no NOE violations were selected and are presented in Figure 4A. NMR and stereochemical parameters for the 20 structures of the ZBD are given in Table 1.

The superposition of the ZBD structures shows excellent agreement with an RMSD to the mean structure of 0.21 ± 0.03 Å for the backbone atoms of residues 2−20 and 0.73 ± 0.05 Å for all heavy atoms (Table 1). The geometry of the structures, as assessed by PROCHECK-NMR, showed that all of the residues were in the favored and allowed

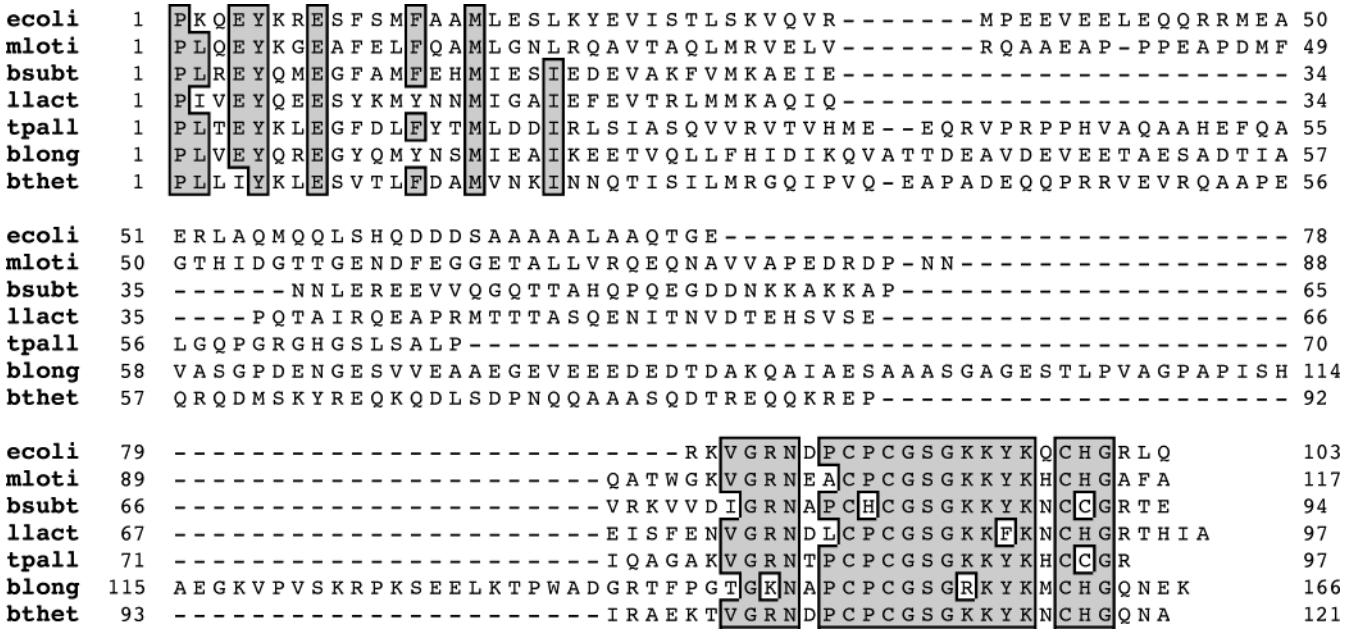

FIGURE 1: Sequence alignment of the C-terminal region of SecA. SecA sequences from 86 bacteria were aligned, and then highly similar sequences were culled from the alignment (see Figure 2 for a phylogenetic tree derived from the alignment). Only the C-terminal region of ZBD-containing SecA molecules is shown; the alignment includes approximately 25 residues of conserved sequence from the main body of the enzyme, which is followed by 60−95 residues of very poorly conserved sequence, ending in the highly conserved zinc-binding domain. In the case of *E. coli*, the first residue shown is Pro799. Note that of the organisms represented in the alignment, only *E. coli* and *M. loti* contain SecB in their genome (see Figure 2). The short names refer to the organisms as follows: ecoli, *Escherichia coli*; mloti, *Mesorhizobium loti*; bsubt, *Bacillus subtilis*; llact, *Lactococcus lactis*; tpall, *Treponema pallidum*; blong, *Bifidobacterium longum*; bthet, *Bacteroides thetaiotamicron*.

regions of the Ramachandran plot, except for Cys19, which falls in a "generously allowed" region.

EXAFS analysis of the Zn^{2+}-ZBD complex (see below) indicated tetrahedral geometry with Zn^{2+}−N and Zn^{2+}−S bond distances of 2.03 and 2.30 Å, respectively. These data were incorporated into our structure calculations by including restraints in the bond distances between the Zn^{2+} atom and its four ligands, as well as restraints between the coordinating atoms. The presence of these additional restraints resulted in only a modest shift in the backbone of the ZBD structure, and, importantly, none of the previously determined NOE restraints were violated. The final structures for the Zn^{2+}-ZBD complex are presented in Figure 4B. Note that several NOE restraints dictate that ligation by His20 is through ND1 and not NE2, consistent with the crystal structural analysis in which ND1 was chosen as the Zn^{2+} ligand (*11*).

What is perhaps most surprising about the collection of NMR structures is their very strong agreement with one another; in other words, the ZBD maintains a tightly folded, compact conformation even when it is free in solution. This relatively high degree of structural stability extends to the N- and C-termini, residues 1−7 and 21−22, even though they are outside of the region directly stabilized by Zn^{2+}. The conformation of the N-terminus, in particular, is backed by NOE data showing a stable interaction between Tyr16 and Val2. The conformation of the N- and C-termini in the solution structure of the ZBD closely resembles that when it is bound to SecB (*11*), indicating that there are no major structural changes when the ZBD interacts with SecB. We have shown that the peptide is completely unfolded in the absence of Zn^{2+}, and, given the lack of regular secondary structure in the ZBD, as well as the absence of a hydrophobic core, it is remarkable that the entire structure is so effectively stabilized by the presence of the Zn^{2+} atom.

We have aligned the ZBD sequences found in the 59 organisms that contain SecA with a ZBD; the nature of the amino acid changes at each position is indicated in Table 2. There are five residues that are perfectly conserved: Cys8, Cys10, Ser12, Gly13, and Cys19; in addition, His20 is only ever replaced by cysteine, and Tyr16 is only ever replaced by phenylalanine, and so these residues exhibit a very high degree of functional conservation. An analysis of the structure (Figure 5) illuminates the role of these conserved residues. First, the NMR structure and the EXAFS analysis (below) indicate that the three cysteines, Cys8, Cys10, Cys19, along with His20, provide the primary coordination for the Zn^{2+} atom; in the sequence alignment of the SecA-ZBDs, there are no insertions or deletions between the Zn^{2+}-ligating residues. Evidently, the compact nature of the ZBD does not allow for any flexibility in the relative positions of the pairs of Zn^{2+}-coordinating residues.

One interesting feature of the ZBD is the strained nature of the interaction between Cys19, His20, and the Zn^{2+} atom. Several NOE restraints fix the conformation of the His20 imidazole ring such that ND1, and not NE2, must be the nitrogen that binds the Zn^{2+} atom. This is somewhat unusual because most structural Zn^{2+} atoms are bound to the NE2 atom of ligating histidine residues, whereas binding by ND1 is more often found in Zn^{2+} metalloenzymes such as carbonic anydrase. *Ab initio* molecular orbital energy calculations indicate that the lowest energy state for Zn^{2+}−imidazole complexes is one in which the Zn^{2+}−N bond bisects the C−N−C bond and is in the same plane as the imidazole ring (*34*); see Figure 6 for conventions. When high-resolution structures of metal−imidazole complexes are analyzed, the

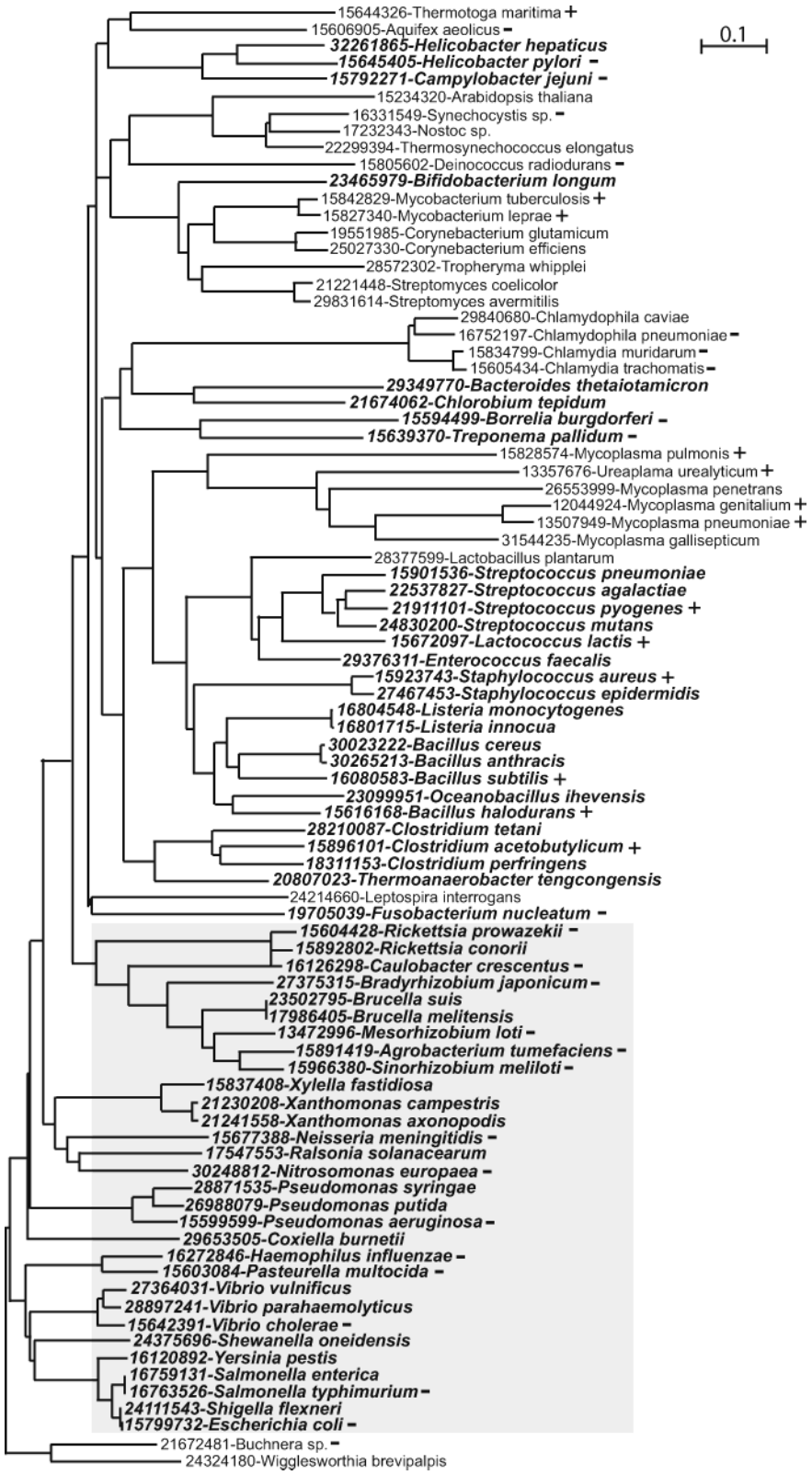

FIGURE 2: Phylogenetic analysis of SecA and SecB. The phylogenetic tree is derived from an alignment of SecA molecules from 86 organisms. The presence of the zinc-binding domain (ZBD) of SecA can be compared with the presence of SecB: organisms with SecB in their genome are indicated by the shaded box, while organisms with a ZBD-containing SecA are shown in bold italics. The bacteria are therefore divided into three groups. Group I organisms possess both a ZBD-containing SecA and SecB. The remainder of the organisms do not carry a gene coding for SecB; however, the Group II organisms carry a ZBD-containing SecA, while the Group III organisms (plain text) carry SecA that lacks the ZBD. To show that the SecA-ZBD is not correlated with the presence of an outer membrane, selected diderm organisms (those with an outer membrane; (*33*, *43*, *44*)) are indicated by a minus sign (they are usually Gram-negative), while selected monoderm organisms are indicated with a plus sign. Note that only selected organisms are indicated with a plus or minus sign because Gram staining is not a completely reliable indicator of whether an organism has an outer membrane, and at the current time a comprehensive list of bona fide diderm and monoderm organisms is not available.

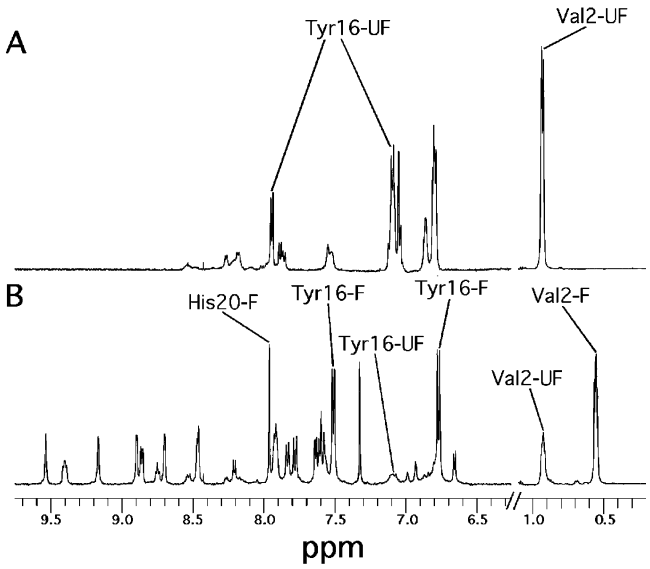

FIGURE 3: Zinc-induced folding of the SecA C-terminal domain. A one-dimensional ^{1}H NMR spectrum of the 22-residue peptide representing the C-terminal zinc-binding domain of SecA was collected in either the absence (A), or the presence (B), of 2 equiv of Zn^{2+}. For the sake of clarity, only the low- and high-field regions are shown. The Zn^{2+}-induced changes in the spectrum are consistent with the peptide changing from an unstructured and rapidly exchanging regime to a folded conformation. A number of resonances in the unfolded form (i.e., for the peptide in the absence of Zn^{2+}) did not fully disappear upon addition of $Zn(OAc)_2$; two of these are illustrated, Val2 and Tyr16 (UF and F refer to the resonances from these residues in the unfolded and folded forms, respectively). Note that in the 1D spectrum of the peptide recorded in the presence of Zn^{2+} (B), a resonance from His20 obscures the peak remaining for the Tyr16 "unfolded" resonance.

bond between the metal and the imidazole nitrogen is, on average, about 5° out-of-plane with the imidazole ring, and the "in-plane" distortion (i.e., the deviation of the $Zn^{2+}-N$ bond from a perfect bisection of the C−N−C bond) is 2−3° (*34*, *35*). In the 20 lowest energy NMR structures, the values for the out-of-plane angle, Θ, ranged from 43° to −5°, with an average value of 17° ± 12° (mean ± s.d.). Using our conventions, the values for Θ in the two ZBDs of the SecB-ZBD complex structure (*11*) are −20° and −23°; in other words, the ligating imidazole ring in the crystal structure is tilted in the opposite direction. The $Zn^{2+}-$imidazole bonds in the 20 lowest-energy NMR structures also had significant in-plane distortions (angle Φ, Figure 6A), tightly clustered around an average value of 13° ± 2° (mean ± s.d.). Regarding the coordination of Zn^{2+} by Cys19 and His20, it is noteworthy that all of the residues in the ZBD structure have favorable main-chain dihedral bond angles, except for Cys19 with $\phi = -150°$ and $\psi = -79°$, which falls in a disallowed region. The distortion in the $Zn^{2+}-$imidazole bond and the strained main-chain ϕ/ψ angles for Cys19 are likely due to the unprecedented situation of having the cysteine and histidine ligands adjacent to each other.

Another interesting feature of the ZBD is the "second sphere" of coordinating interactions. That is, the three thiolates bind the Zn^{2+} atom, and they also participate in hydrogen-bonding interactions with other groups on the peptide, further stabilizing the structure. The thiolates of Cys8 and Cys10 are positioned to accept hydrogen bonds from the main-chain NH groups of residues His20 and Ser12, respectively. Most interesting is the situation with Cys19 and its relationship with Ser12: Ser12 is one of the perfectly conserved residues, and the NMR structure suggests an important functional role for its side chain. When the side chain adopts a χ^1 value of 70° (which corresponds to the predominant rotamer populated by serine residues), the alcohol moiety points into the interior of the ZBD and is able to accept a hydrogen bond from the main-chain amide of Lys14 and donate a hydrogen bond to the thiolate of Cys19. Thus, Ser12 mediates a hydrogen-bonding interaction between the thiolate of Cys19 and the amide of residue 14, thereby stabilizing the main-chain structure around the Zn^{2+} atom. The strength of this interaction is borne out by the NMR data, which show the OG proton of Ser12 in slow exchange and having NOEs to its own CB protons, the CB protons of Cys8, Cys19, and Lys14, the CA protons of G11, and the main-chain amide protons of Ser12, Gly13, and Lys14. This indicates that the hydrogen bond between Ser12 and Cys19 is exceptionally stable.

The other conserved residues are Gly13 and Tyr16. The backbone ϕ and φ angles of Gly13 are 127° and −29°, respectively, and therefore a change in the backbone structure would be required to accommodate any other residue in that position. One effect of a change in the backbone conformation in this region would be to compromise the ability of the NH group of Lys14 to make a strong hydrogen bond with OG of Ser12.

Tyr16, which is sometimes replaced by Phe, provides the only "hydrophobic core" of the ZBD: it contacts CA of Gly21, the side-chain carbons of Val2, which is usually a hydrophobic residue in the ZBD sequences, and the side-chain carbons of Pro9, which is also highly conserved. The edge of Tyr16 also makes contact with the thiolate of Cys8; although the exact nature of this interaction is not clear, the presence of a conserved aromatic amino acid next to metal-coordinating residues has been noted previously and has been shown to be important for metal-dependent folding (*36*). The numerous NOEs between Tyr16 and other residues, particularly Val2, indicate that it is the central and most important residue in maintaining the conformation of the N-terminal amino acids.

X-ray Absorption Analysis of the Zinc-Binding Domain. The NMR structure obtained in the absence of any restraints between the Zn^{2+} atom and the peptide was consistent with Zn^{2+}-coordination by Cys8, Cys10, Cys19, and His20, although when a Zn^{2+} atom was modeled into the structure, the bond distances and coordination geometry appeared to be somewhat distorted; furthermore, it seemed possible that a water molecule could also interact with the Zn^{2+} atom, yielding pentavalent coordination. Because of the unusual sequence of the ZBD, and in particular the spacing of the putative Zn^{2+} ligands, we characterized the environment around the metal ion using X-ray absorption spectroscopic analysis to ensure that the $Zn^{2+}-$peptide restraints we applied to the NMR structure were justified.

The X-ray absorption near edge structure (XANES) spectra of $Zn^{2+}-$peptides are sensitive to the number of coordinating sulfur and nitrogen atoms and can be used to characterize the Zn^{2+} ligation (*37*, *38*). The first XANES peak corresponds to the 1s → 4p transition and is sensitive to the coordination geometry around the Zn^{2+} site (*39*): an intense peak is an indicator for Zn^{2+} being in a 5-coordinated environment, while it is generally weaker in 4-coordinated

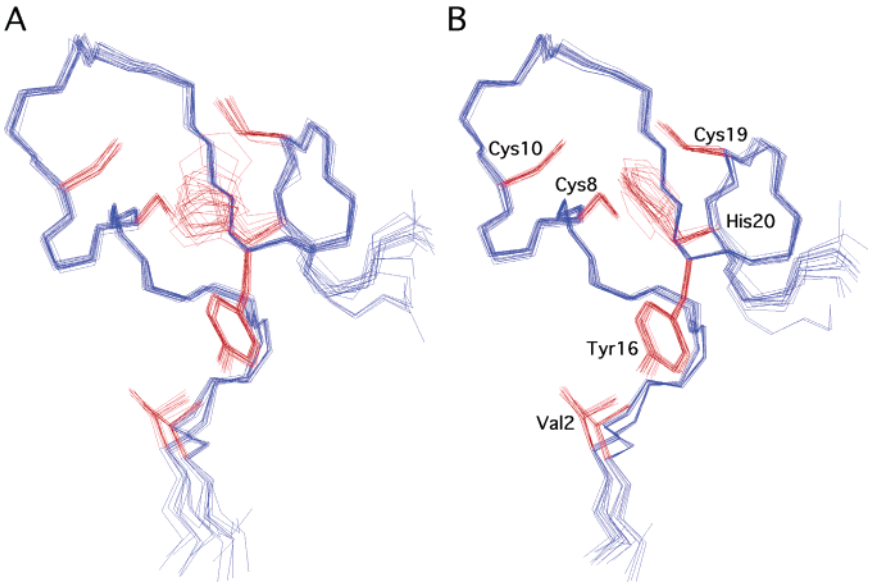

FIGURE 4: Structures of the SecA-ZBD determined by NMR spectroscopy. The 20 lowest energy structures determined for the Zn^{2+}−ZBD complex, calculated with (A) the NMR data alone, or (B) the NMR data along with Zn^{2+}−S and Zn^{2+}−N bond distance restraints and tetrahedral geometry restraints, as determined from EXAFS analysis. In each case, 100 structures for the ZBD were calculated by CNS (*27*), and the 20 lowest energy structures were selected; these structures were superimposed using the backbone atoms of residues 2−20, which are relatively well structured. The structure parameters for these models are presented in Table 1. Selected functionally important residues are highlighted in red; these include the Zn^{2+} ligands Cys8, Cys10, Cys19, and His20, as well as Val2 and Tyr16 which are important for maintaining the structure of the 7 N-terminal residues. The figure was produced with MOLMOL (*45*).

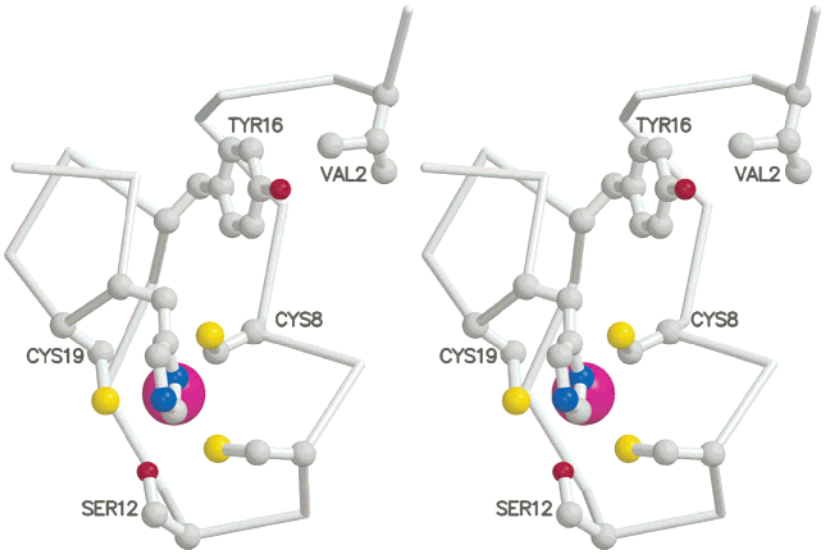

FIGURE 5: Structural features of the SecA-ZBD. A stereoview of the overall fold and highly conserved side chains of the SecA-ZBD. Val2 and Tyr16 interact, stabilizing the N-terminal residues. The Zn^{2+} ligands are Cys8, Cys10, Cys19, and His20; note that ND1 was identified as the nitrogen bound to the Zn^{2+} atom and that the Zn^{2+}−ND1 bond makes an angle of approximately 17° with the plane of the imidazole ring. Ser12 makes a hydrogen bond with Cys19. The figure was produced using Molscript (*46*) and Raster3D (*47*).

Zn^{2+} complexes (*38*). The observed XANES spectrum of the SecA-ZBD, in which a strong peak at approximately 9663 eV is absent, is therefore consistent with a 4-coordinated Zn^{2+} (Figure 7A).

The extended X-ray absorption fine structure (EXAFS) spectrum for the Zn^{2+}-ZBD was analyzed over a wide *k*-range, $2 < k < 15.1$ Å^{-1}. The corresponding Fourier transform (Figure 7B, distances not corrected for phase shift) displays a major peak at 1.9 Å with a shoulder around 1.6 Å, which is consistent with Zn^{2+}−S_3N coordination (*37*). The small peak at 2.7 Å can be attributed to the outer shell backscattering between Zn^{2+} and the imidazole ring carbon atoms.

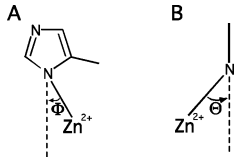

FIGURE 6: Geometry of the Zn^{2+}−imidazole bond. In addition to its length, the Zn^{2+}−N bond is characterized by its relationship to the imidazole ring using two parameters, Φ and Θ, as defined in Carrell *et al.* (*34*). (A) The in-plane distortion (angle Φ), which refers to the angle between the Zn^{2+}−N bond and the line that bisects the imidazole ring C−N−C bond angle (dashed line). (B) The out-of-plane distortion (angle Θ), which is defined by the angle that the Zn^{2+}−N bond makes with the plane of the imidazole ring.

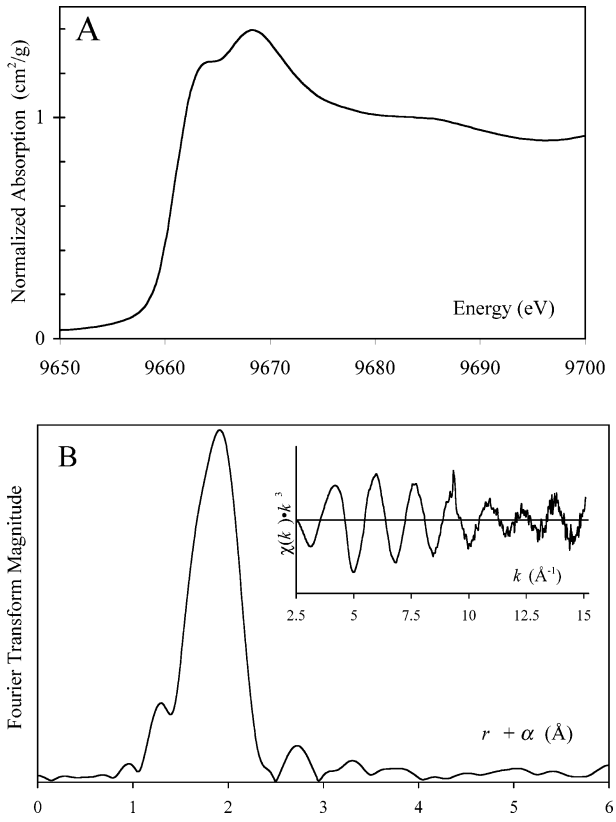

FIGURE 7: X-ray absorption analysis of the SecA-ZBD. (A) Normalized Zn XANES spectrum of the Zn^{2+}-ZBD. Note the absence of a strong first peak at approximately 9663 eV, which is consistent with a four-cooordinated Zn^{2+} (*38*). (B) The k^3-weighted Zn^{2+} K-edge EXAFS spectrum (inset) and corresponding Fourier transform for the Zn^{2+}-ZBD over the range $k = 2.5-15.1$ Å^{-1}.

The Fourier transform shows that the Zn^{2+} EXAFS oscillation is dominated by the direct backscattering from the atoms in the first coordination shell. We used the NMR-derived structural model of the SecA-ZBD for calculations of the EXAFS oscillations (see Experimental Procedures); in the lowest-energy SecA-ZBD model, the three cysteine thiolate sulfur atoms are at 2.36 Å from the Zn^{2+}, and ND1 of the imidazole ring is at 2.10 Å from the Zn^{2+}. Least-squares refinements of a few structural parameters, such as the coordination distance, *R*, and the Debye−Waller parameter, σ^2, were performed by fitting the model oscillations to the experimental EXAFS data. The least-squares curve fitting can be made on the "raw" (unfiltered) data, or on Fourier-filtered EXAFS curves, which are obtained by eliminating peaks from long distances and physically unreasonable peaks at low *r*-values. Fitting either the raw or the filtered experimental data with the ZBD model consistently yielded $Zn^{2+}-N$ and $Zn^{2+}-S$ distances of 2.03 and 2.30 Å, respectively (Table 3), in accordance with the restraints we imposed for the structure determination.

The Debye−Waller parameter, σ^2, provides a measure of the mean-square vibrational displacements together with the static disorder of the backscattering atoms. Refinement of unfiltered data resulted in an unreasonably low σ^2 value for $Zn^{2+}-N$, and it was therefore fixed at 4×10^{-4} (Table 3, fit #4), which represents the value obtained from fitting the filtered data in a similar *k*-range (Table 3, fit #1). When the model was fit using lower *k*-ranges (Table 3, fits #2 and #3), the Debye−Waller parameter refined to a more reasonable value of 2.0; in these cases, the Debye−Waller parameter for the $Zn^{2+}-N$ bond distance showed a correlation with the amplitude reduction factor (S_0^2), probably because of the noise level in the high *k*-range (Figure 8), and therefore S_0^2 was fixed at 1.00 for the refinement using a restricted *k*-range ($k_{max} < 13$ Å^{-1}; Table 3, fit #3). Thus, the unreasonably low Debye−Waller parameter for the $Zn^{2+}-N$ bond appears to have its origin in the high *k*-range data; note that use of a *k*-range under 13 Å^{-1} is typical for aqueous solutions of peptides or proteins (*37*). The higher σ^2 value for $Zn^{2+}-S$ as compared to that for $Zn^{2+}-N$ indicates that there is a distribution of the three Zn−S bond distances around the mean value of 2.30 Å.

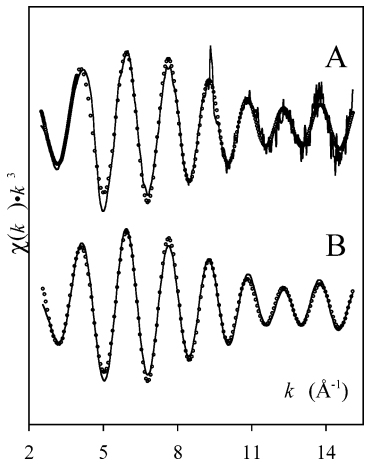

FIGURE 8: Model fitting to EXAFS data. Curve fittings of k^3-weighted Zn^{2+} K-edge EXAFS using the Zn^{2+}-ZBD model. The experimental EXAFS, either unfiltered (A) or Fourier-filtered (B), is shown as solid curves. The model-derived theoretical EXAFS is plotted using hollow circles. (A) The fit of the Zn^{2+}-ZBD model to the raw data (fit #4, Table 3). (B) Fit of the Zn^{2+}-ZBD model to the Fourier-filtered data (fit #1, Table 3).

To summarize, the SecA-ZBD model derived from NMR is consistent with the EXAFS data that indicate tetrahedral coordination, with a mean $Zn^{2+}-S$ distance of 2.30 Å and a $Zn^{2+}-N$ distance of 2.03 Å.

Complex Folding of the SecA-ZBD. When Zn^{2+}-induced folding is followed using NMR, it is apparent that some resonances representing the unfolded conformation of the peptide do not completely disappear upon addition of saturating amounts of Zn^{2+}. For example, the well-resolved resonances for the methyl protons of Val2 at 0.92 ppm and the ring protons of Tyr16 at 7.10 and 7.95 ppm in the unfolded peptide recorded in the absence of Zn^{2+} (Figure 3A) are present even after the addition of 2 equiv of Zn^{2+}. Analysis of the peak integrals shows that the Zn^{2+}-induced conversion to the fully folded conformation occurs for approximately 60% of the peptide. All of the well-resolved resonances can be accounted for by the one fully folded conformation, and therefore the fraction that does not adopt this conformation appears to remain largely unfolded. In addition, resonances for the unfolded form of the ZBD had minimal NOE contacts, consistent with an unstructured conformation.

Our first thought was that a fraction of the peptide was not folding properly because of the presence of an inter- or intramolecular disulfide bond. To investigate this possibility, we measured the mass of the peptide after the NMR

experiments by ESI-MS, and we found that the molecular weight, 2459.3 ± 0.5 Da, corresponded with the fully reduced form (theoretical M_R 2459.2 Da); furthermore, the mass spectrum recorded after the NMR experiments showed no significant differences from that of the newly synthesized peptide. Preliminary experiments in which the temperature and pH were altered, as well as the quantity and rate of addition of Zn^{2+}, had no effect on the fraction of peptide that adopted the fully folded conformation. Although at this point the exact nature of the unfolded ZBD is not known, it does not contribute in a significant way to the experimental NMR spectra, and therefore our structure determination of the fully folded Zn^{2+}-bound peptide is not affected. We intend to more fully characterize the folding of the SecA-ZBD in subsequent studies.

DISCUSSION

We have solved the solution NMR structure of a novel zinc-binding domain (ZBD) found on the SecA subunit of preprotein translocase from *Escherichia coli*, and details of the immediate environment around the Zn^{2+} atom were elucidated using X-ray absorption analysis. A crystal structure of this domain was revealed first in a complex between it and the translocase-specific chaperone, SecB, both from *H. influenzae* (*11*). A comparison between the two structures shows that the conformation of the N- and C-terminal residues does not change when the ZBD binds SecB; this is somewhat surprising given the fact that the Zn^{2+} ligands, C8, C10, C19, and H20, span only half of the peptide. The NMR-derived model differs from the crystal structure in several important aspects: in the conformation of the His20 side chain, the main-chain conformation between Pro9 and Cys10, and the conformation of the Ser12 side chain.

The SecA-ZBD has an unusual and highly conserved sequence; in particular, two of the Zn^{2+} ligands, Cys19 and His20, are adjacent to each other. The presence of adjacent Zn^{2+}-binding residues has been observed in one other protein, RNA polymerase subunit RPB10 (*40*), but in RPB10, the adjacent Zn^{2+} ligands are both cysteine residues. It would appear from the NMR structure that the adjacent position of the Cys−His Zn^{2+} ligands is less than optimal: the main-chain dihedral angles between the two residues fall in a disallowed region of the Ramachandran plot, and, although the side chain of His20 adopts a conformation that corresponds to a well-populated rotamer (*41*), the bond between the Zn^{2+} atom and ND1 of the imidazole ring is not ideal, with a large out-of-plane angle, Θ, of 17° and an in-plane angle, Φ, of 13°.

The alignment of 59 ZBD sequences indicates that, in addition to absolute conservation of the Zn^{2+} ligands, the ZBD motif of SecA also has a perfectly conserved serine residue. The NMR data indicate that the OG proton of Ser12 is slowly exchanging and must therefore be participating in a strong hydrogen bond, likely with the thiolate of Cys19. The side chain of Ser12 is also in a good position to accept a hydrogen bond from the main-chain amide of Lys14. Given its high sequence conservation and strong hydrogen-bonding interaction, it appears that Ser12 plays a critical role in the folding and stability of the ZBD. Similar second-sphere interactions have been observed in betaine-homocysteine methyltransferase (BHMT (*42*)). For BHMT, there is a Cys−His (Cys217−His218) sequence, but in the crystal structure of the reduced form of the enzyme, a Zn^{2+} is ligated by Cys217 and two other cysteine residues, plus a homocysteine substrate analogue (*42*). The histidine in this case does not directly bind the Zn^{2+} ion, but instead may function as a second-sphere ligand, donating a hydrogen bond to the thiolate of Cys217. Interestingly, the thiolate of Cys217 also makes contact with a nearby tyrosine residue (Tyr160), reminiscent of the interaction between Cys8 and Tyr16 in the SecA-ZBD structure.

The NMR analysis shows that the Zn^{2+}-binding site is not preformed, but instead the ZBD polypeptide must fold as it binds Zn^{2+}. This folding process is complicated by the presence of two proline residues in the sequence, at positions 7 and 9. In particular, Pro9, which is situated between the Zn^{2+} ligands Cys8 and Cys10, may cause problems with folding if the Pro9−Cys10 bond adopts a *cis* conformation. We have found that there are two conformers that can be separated by RP-HPLC (data not shown), all of which have identical molecular weights corresponding to the reduced form of the polypeptide. These conformational isomers are most likely the result of one or more *cis* prolyl peptide bonds. With respect to the NMR analysis, we have found that a significant fraction of the polypeptide appears to remain unfolded when a large excess of Zn^{2+} is added. One possible explanation for these results is that higher concentrations of excess Zn^{2+} are able to stabilize the *cis* prolyl bonds that could exist in subpopulations of the peptide, slowing or preventing the folding of these fractions. We intend to investigate further the kinetics of folding of the ZBD, as well as the role of Ser12 in folding and stability.

Finally, we believe the SecA-ZBD has roles other than simply binding to SecB. A phylogenetic analysis indicates that in almost half of the organisms that carry a ZBD-containing SecA, there is no gene coding for SecB. It may be that there is another export-specific chaperone in these organisms and that the ZBD mediates an interaction with this chaperone in a manner similar to that of the SecA−SecB interaction. Alternatively, the SecA-ZBD may have other, as yet uncharacterized binding partners in all genomes in which it is found.

ACKNOWLEDGMENT

We thank Prof. Radhey Gupta for useful discussions. We gratefully acknowledge the beam time and the staff support provided at the Photon Factory, with special thanks to Prof. Masaharu Nomura. Thanks are also due to the Alberta Synchrotron Institute for supporting the BioXAS project at the University of Calgary.

REFERENCES

1. Brundage, L., Hendrick, J. P., Schiebel, E., Driessen, A. J., and Wickner, W. (1990) The purified *E. coli* integral membrane protein SecY/E is sufficient for reconstitution of SecA-dependent precursor protein translocation, *Cell 62*, 649−657.
2. Economou, A., and Wickner, W. (1994) SecA promotes preprotein translocation by undergoing ATP-driven cycles of membrane insertion and deinsertion, *Cell 78*, 835−843.
3. Hartl, F.-U., Lecker, S., Schiebel, E., Hendrick, J. P., and Wickner, W. (1990) The binding cascade of SecB to SecA to SecY/E mediates preprotein targeting to the *E. coli* plasma membrane, *Cell 63*, 269−279.

4. Kim, J., Miller, A., Wang, L., Muller, J. P., and Kendall, D. A. (2001) Evidence that SecB enhances the activity of SecA, *Biochemistry 40*, 3674−3680.
5. Miller, A., Wang, L., and Kendall, D. A. (2002) SecB modulates the nucleotide-bound state of SecA and stimulates ATPase activity, *Biochemistry 41*, 5325−5332.
6. Breukink, E., Nouwen, N., van Raalte, A., Mizushima, S., Tommassen, J., and de Kruijff, B. (1995) The C terminus of SecA is involved in both lipid binding and SecB binding, *J. Biol. Chem. 270*, 7902−7907.
7. Fekkes, P., van der Does, C., and Driessen, A. J. (1997) The molecular chaperone SecB is released from the carboxy-terminus of SecA during initiation of precursor protein translocation, *EMBO J. 16*, 6105−6113.
8. Fekkes, P., de Wit, J. G., Boorsma, A., Friesen, R. H., and Driessen, A. J. (1999) Zinc stabilizes the SecB binding site of SecA, *Biochemistry 38*, 5111−5116.
9. Hunt, J. F., Weinkauf, S., Henry, L., Fak, J. J., McNicholas, P., Oliver, D. B., and Deisenhofer, J. (2002) Nucleotide control of interdomain interactions in the conformational reaction cycle of SecA, *Science 297*, 2018−2026.
10. Sharma, V., Arockiasamy, A., Ronning, D. R., Savva, C. G., Holzenburg, A., Braunstein, M., Jacobs, W. R., Jr., and Sacchettini, J. C. (2003) Crystal structure of *Mycobacterium tuberculosis* SecA, a preprotein translocating ATPase, *Proc. Natl. Acad. Sci. U.S.A. 100*, 2243−2248.
11. Zhou, J., and Xu, Z. (2003) Structural determinants of SecB recognition by SecA in bacterial protein translocation, *Nat. Struct. Biol. 10*, 942−947.
12. Gannon, P. M., and Kumamoto, C. A. (1993) Mutations of the molecular chaperone protein SecB which alter the interaction between SecB and maltose-binding protein, *J. Biol. Chem. 268*, 1590−1595.
13. Kimsey, H. H., Dagarag, M. D., and Kumamoto, C. A. (1995) Diverse effects of mutation on the activity of the *Escherichia coli* export chaperone SecB, *J. Biol. Chem. 270*, 22831−22835.
14. Karlin, S., and Zhu, Z. Y. (1997) Classification of mononuclear zinc metal sites in protein structures, *Proc. Natl. Acad. Sci. U.S.A. 94*, 14231−14236.
15. Altschul, S. F., Madden, T. L., Schaffer, A. A., Zhang, J., Zhang, Z., Miller, W., and Lipman, D. J. (1997) Gapped BLAST and PSI-BLAST: a new generation of protein database search programs, *Nucleic Acids Res. 25*, 3389−3402.
16. Katoh, K., Misawa, K., Kuma, K., and Miyata, T. (2002) MAFFT: a novel method for rapid multiple sequence alignment based on fast Fourier transform, *Nucleic Acids Res. 30*, 3059−3066.
17. Thompson, J. D., Higgins, D. G., and Gibson, T. J. (1994) CLUSTAL W: improving the sensitivity of progressive multiple sequence alignment through sequence weighting, position-specific gap penalties and weight matrix choice, *Nucleic Acids Res. 22*, 4673−4680.
18. Piantini, U., Sorensen, O. W., and Ernst, R. R. (1982) Multiple quantum filters for elucidating NMR coupling networks, *J. Am. Chem. Soc. 104*, 6800−6801.
19. Bax, A., and Davis, D. G. (1985) MLEV-17 based two-dimensional homonuclear magnetization transfer spectroscopy, *J. Magn. Reson. 65*, 355−360.
20. States, D. J., Haberkorn, R. A., and Rubin, D. J. (1982) A two-dimensional nuclear Overhauser experiment with pure absorption phase in four quadrants, *J. Magn. Reson. 48*, 286−292.
21. Delaglio, F., Grzesiek, S., Vuister, G. W., Zhu, G., Pfeifer, J., and Bax, A. (1995) NMRPipe: A multidimensional spectral processing system based on UNIX pipes, *J. Biomol. NMR 6*, 277−293.
22. Gagne, S. M., Tsuda, S., Li, M. X., Chandra, M., Smillie, L. B., and Sykes, B. D. (1994) Quantification of the calcium-induced secondary structural changes in the regulatory domain of troponin-C, *Protein Sci. 3*, 1961−1974.
23. Karplus, M. (1959) Contact electron-spin coupling of nuclear magnetic moments, *J. Chem. Phys. 30*, 11−15.
24. Pardi, A., Billeter, M., and Wuthrich, K. (1984) Calibration of the angular dependence of the amide proton-C alpha proton coupling constants, 3JHN alpha, in a globular protein. Use of 3JHN alpha for identification of helical secondary structure, *J. Mol. Biol. 180*, 741−751.
25. Cornilescu, G., Delagio, F., and Bax, A. (1999) Protein backbone angle restraints from searching a database for chemical shift and sequence homology, *J. Biomol. NMR 13*, 289−302.
26. Wagner, G., Braun, W., Havel, T. F., Schaumann, T., Go, N., and Wuthrich, K. (1987) Protein structures in solution by nuclear magnetic resonance and distance geometry, *J. Mol. Biol. 196*, 611−639.
27. Brunger, A. T., P. D., A., Clore, G. M., DeLano, W. L., Gros, P., Grosse-Kunstleve, R. W., Jiang, J.-S., Kuszewski, J., Nilges, M., Pannu, N. S., Read, R. J., Rice, L. M., Simonson, T., and Warren, G. L. (1998) Crystallography & NMR system: A new software suite for macromolecular structure determination, *Acta Crystallogr. D54*, 905−921.
28. Berman, H. M., Westbrook, J., Feng, Z., Gilliland, G., Bhat, T. N., Weissig, H., Shindyalov, I. N., and Bourne, P. E. (2000) The protein data bank, *Nucleic Acids Res. 28*, 235−242.
29. Ressler, T. (1998) WinXAS: a program for X-ray absorption spectroscopy data analysis under MS-Windows, *J. Synchrotron Radiat. 5*, 118−122.
30. Zabinsky, S. I., Rehr, J. J., Ankudinov, A. L., Albers, R. C., and Eller, M. J. (1995) Multiple-scattering calculations of X-ray absorption spectra, *J. Phys. Rev. B52*, 2995−3009.
31. Kumamoto, C. A., and Francetic, O. (1993) Highly selective binding of nascent polypeptides by an *Escherichia coli* chaperone protein in vivo, *J. Bacteriol. 175*, 2184−2188.
32. Lill, R., Cunningham, K., Brundage, L., Ito, K., Oliver, D., and Wickner, W. (1989) The SecA protein hydrolyzes ATP and is an essential component of the protein translocation ATPase of *E. coli*, *EMBO J. 8*, 961−966.
33. Gupta, R. S. (1998) Protein phylogenies and signature sequences: A reappraisal of evolutionary relationships among archaebacteria, eubacteria, and eukaryotes, *Microbiol. Mol. Biol. Rev. 62*, 1435−1491.
34. Carrell, A. B., Shimoni, L., Carrell, C. J., Bock, C. W., Murray-Rust, P., and Glusker, J. P. (1993) The stereochemistry of the recognition of nitrogen-containing heterocycles by hydrogen bonding and by metal ions, *Receptor 3*, 57−76.
35. Harding, M. M. (1999) The geometry of metal−ligand interactions relevant to proteins, *Acta Crystallogr. D55*, 1432−1443.
36. Opella, S. J., DeSilva, T. M., and Veglia, G. (2002) Structural biology of metal-binding sequences, *Curr. Opin. Chem. Biol. 6*, 217−223.
37. Clark-Baldwin, K., Tierney, D. L., Govindaswamy, N., Gruff, E. S., Kim, C., Berg, J., Koch, S. A., and Penner-Hahn, J. E. (1998) The limitations of X-ray absorption spectroscopy for determining the structure of zinc sites in proteins. When is a tetrathiolate not a tetrathiolate, *J. Am. Chem. Soc. 120*, 8401−8409.
38. Jacquamet, L., Aberdam, D., Adrait, A., Hazemann, J. L., Latour, J. M., and Michaud-Soret, I. (1998) X-ray absorption spectroscopy of a new zinc site in the fur protein from *Escherichia coli*, *Biochemistry 37*, 2564−2571.
39. Koningsberger, D. C., and Prins, R. (1988) *X-ray absorption: principles, applications, techniques of EXAFS, SEXAFS and XANES*, J. Wiley, New York; Toronto.
40. Mackereth, C. D., Arrowsmith, C. H., Edwards, A. M., and McIntosh, L. P. (2000) Zinc-bundle structure of the essential RNA polymerase subunit RPB10 from Methanobacterium thermoautotrophicum, *Proc. Natl. Acad. Sci. U.S.A. 97*, 6316−6321.
41. Ponder, J. W., and Richards, F. M. (1987) Tertiary templates for proteins. Use of packing criteria in the enumeration of allowed sequences for different structural classes, *J. Mol. Biol. 193*, 775−791.
42. Evans, J. C., Huddler, D. P., Jiracek, J., Castro, C., Millian, N. S., Garrow, T. A., and Ludwig, M. L. (2002) Betaine-homocysteine methyltransferase: zinc in a distorted barrel, *Structure 10*, 1159−1171.
43. Gupta, R. S. (2000) The natural evolutionary relationships among prokaryotes, *Crit. Rev. Microbiol. 26*, 111−131.
44. Gupta, R. S. (2001) The branching order and phylogenetic placement of species from completed bacterial genomes, based on conserved indels found in various proteins, *Int. Microbiol. 4*, 187−202.
45. Koradi, R., Billeter, M., and Wuthrich, K. (1996) MOLMOL: a program for display and analysis of macromolecular structures, *J. Mol. Graphics 14*, 29−32, 51−55.
46. Kraulis, P. (1991) MOLSCRIPT: a program to produce both detailed and schematic plots of protein structures, *J. Appl. Crystallogr. 24*, 946−950.
47. Merritt, E. A., and Bacon, D. J. (1997) Raster3D: photorealistic molecular graphics, *Methods Enzymol. 277*, 505−524.

BI0493057